Available online at www.sciencedirect.com
SCIENCE DIRECT®
ELSEVIER
Nuclear Instruments and Methods in Physics Research A 548 (2005) 364–374
NUCLEAR INSTRUMENTS & METHODS IN PHYSICS RESEARCH Section A
www.elsevier.com/locate/nima

The aerogel threshold Cherenkov detector for the High Momentum Spectrometer in Hall C at Jefferson Lab

R. Asaturyan[a,*], R. Ent[b], H. Fenker[b], D. Gaskell[b], G.M. Huber[c], M. Jones[b], D. Mack[b], H. Mkrtchyan[a], B. Metzger[b], N. Novikoff[d], V. Tadevosyan[a], W. Vulcan[b], S. Wood[b]

[a] *Yerevan Physics Institute, Yerevan 375036, Armenia*
[b] *Thomas Jefferson National Accelerator Facility, Newport News, VA 23606, USA*
[c] *Department of Physics, University of Regina, Regina, SK, Canada S4S 0A2*
[d] *Houston Baptist University, Houston, TX 77074, USA*

Received 19 November 2004; received in revised form 31 March 2005; accepted 1 April 2005
Available online 6 June 2005

Abstract

We describe a new aerogel threshold Cherenkov detector installed in the HMS spectrometer in Hall C at Jefferson Lab. The Hall C experimental program in 2003 required an improved particle identification system for better identification of $\pi/K/p$, which was achieved by installing an additional threshold Cherenkov counter. Two types of aerogel with $n = 1.030$ and $n = 1.015$ allow one to reach $\sim 10^{-3}$ proton and 10^{-2} kaon rejection in the 1–5 GeV/c momentum range with pion detection efficiency better than 99% (97%). The detector response shows no significant position dependence due to a diffuse light collection technique. The diffusion box was equipped with 16 Photonis XP4572 photo multiplier tubes (PMTs). The mean number of photo-electrons in saturation was ~16 and ~8, respectively. This allows even for separation of slower particles slightly above threshold.

PACS: 29.40.Ka; 25.30.Rw

Keywords: Particle identification; Aerogel; Diffusion box; Photoelectron

1. Introduction

The aerogel detector described in this paper was designed and built for experiments carried out in Hall C at Jefferson Laboratory.

A number of (e, e′h) experiments, where a scattered electron is measured in coincidence with

*Corresponding author.
E-mail address: asatur@jlab.org (R. Asaturyan).

0168-9002/$ - see front matter © 2005 Elsevier B.V. All rights reserved.
doi:10.1016/j.nima.2005.04.058

a hadron, have been performed in Hall C since 1995. The Hall C base experimental equipment consists of two magnetic spectrometers, the High Momentum Spectrometer (HMS) and the Short Orbit Spectrometer (SOS) [1]. Depending on the specific requirements of the experiments, one can detect either negatively charged (mostly electrons) or positively charged particles by choosing the proper polarity of the magnetic field and the trigger configuration.

The HMS is designed to detect secondary products of reactions in the momentum range from 0.5 to 7.3 GeV/c, while the SOS momentum extends only up to $\sim$1.7 GeV/c. Both spectrometers are equipped with a pair of drift chambers and X–Y timing scintillator hodoscope planes for trigger formation.

For particle identification (PID), a combination of Time-of-Flight (TOF), threshold gas Cherenkov counter and segmented lead–glass electromagnetic calorimeter (EC) is used. In addition, for coincidence measurements, use of the coincidence time difference between scattered electrons and different types of secondary hadrons is very efficient. But even with perfectly tuned hodoscope arrays and calibrated detectors, in such a configuration $\pi/K/p$ separation dramatically deteriorates with momentum as $\Delta t \sim 1/P^2$. While TOF is very effective at low momentum, it becomes in practice useless above $P \sim 3$ GeV/c. In addition, up to the highest momentum setting of the Hall C HMS neither kaons nor protons will trigger on an atmospheric gas Cherenkov detector. Although pions will trigger on a gas Cherenkov from roughly 3 GeV/c momentum (for C_4F_{10} gas), initial light output will be too low for meaningful π/K separation. Thus, the HMS PID system needs to be augmented for good hadron identification above 3 GeV/c.

A series of Hall C experiments ran in the summer of 2003 that required such an improvement of the HMS PID system. The purpose of the "Baryon Resonance Electroproduction at High Momentum Transfer" [2] experiment was to measure inelastic nucleon transition amplitudes to the $\Delta(1232)$ and $S_{11}(1536)$ baryon resonances via the $p(e,e'p)\pi^\circ$ and $p(e,e'p)\eta$ reactions, respectively, at the momentum transfer of $Q^2 = 7.5\,(\mathrm{GeV}/c)^2$. The scattered electrons were detected in the SOS in coincidence with recoil protons of up to $\sim$5 GeV/c momentum in the HMS. In this experiment, it was important to suppress high-momentum pions with respect to protons.

A second experiment, termed "The Charged Pion Form Factor", measured the pion form factor at $Q^2 = 1.6$ and $2.5\,(\mathrm{GeV}/c)^2$ [3]. In this experiment, one detected pions and electrons in coincidence from the reactions $e + p \to e' + \pi^+ + n$ and $e + d \to e' + \pi^- + p + p$ or $e + d \to e' + \pi^+ + p + n$ (in order to estimate contributions from background physics processes). Here, the HMS was set up for pion detection. At the highest momentum setting of this experiment, $P_{\mathrm{HMS}} \sim 3.4$ GeV/c, the ratio of π^+ to protons was expected to be $\sim$1 and good proton rejection became important.

Finally, the experiment "Duality in Meson Electroproduction" checked the low-energy cross-section factorization and the quark–hadron duality phenomenon in semi-inclusive electroproduction of pions (kaons) [4]. Here, it was important to identify kaons and pions at a momentum $P_{\mathrm{HMS}} \geqslant 3$ GeV/c.

The general requirement for these three experiments was a high detection efficiency for pions in the HMS and the capability to separate protons from pions in the first two cases, and pions from kaons in the third case.

The experiments were planned to run at an electron beam intensity up to 90 μA, hitting a liquid hydrogen (or deuterium) target with a length of 4 cm, yielding rates as high as 1 MHz.

To keep the HMS standard detector configuration intact and not to compromise on HMS performance, the new PID detector should be designed with the following restrictions:

- have a large sensitive area to match HMS spectrometer acceptance, with an effective area of $\sim$1 m^2;
- be slim to fit in an $\sim$25 cm slot in-between the second drift chamber and first hodoscope, the only readily available space in the HMS detector stack;

- have minimum material on the particle path to keep the amount of multiple scattering and δ-electrons small;
- have reasonable time resolution and high rate capability.

To obtain a proton threshold momentum of 3–4.6 GeV/c, for Cherenkov radiation, a medium with index of refraction $n = 1.02$–1.06 is needed. Aerogel is the best candidate for this purpose.

The use of aerogel for PID was first demonstrated by Cantin [5], who observed 6–12 photo-electrons in a volume of $18 \times 18 \times 18\,\mathrm{cm}^3$ for hadrons with $1 \leqslant \gamma \leqslant 5$. Since then many different types of aerogel detectors have been used in physics experiments, but few of them cover the wide acceptance in high-intensity beam experiments we were looking for. Therefore we designed a new device. Two types of aerogel material with different indices of refraction were used.

2. Choice of aerogel radiators

The operation of Cherenkov counters is governed by the basic relation [6,7] which connects the emission angle θ of Cherenkov photons, the velocity $v = \beta c$ of a charged particle and the index of refraction n of the radiator medium. The minimum momentum at which a particle of mass M will exceed the phase velocity of light in the medium is simply given by

$$P_{\min} c = \frac{Mc^2}{\sqrt{n^2 - 1}} \tag{1}$$

where c is the speed of light in vacuum. The number of photons produced by a $Z = 1$ particle per unit track length in a wavelength region between λ_1 and λ_2 depends on the velocity of the particle and the refractive index $n(\lambda)$ of the radiator:

$$\frac{\mathrm{d}N}{\mathrm{d}l} = 2\pi\alpha\left(1 - \frac{1}{n^2(\lambda)\beta^2}\right)\left(\frac{1}{\lambda_1} - \frac{1}{\lambda_2}\right). \tag{2}$$

For the weak variation of n with λ in most of the cases, Eq. (2) is a good approximation.

The number of Cherenkov photons scales as $L \sin^2\theta$, giving a total of N photons produced for a radiator of length L:

$$N = N_0 L \sin^2\theta \tag{3}$$

where

$$N_0 = 2\pi\alpha\left(\frac{1}{\lambda_1} - \frac{1}{\lambda_2}\right) \tag{4}$$

and α is the fine structure constant.

For a diffuse light box having reflectivity M and photodetectors which cover an areal fraction ε of the surface, the average number of photons hitting the PMTs is [8,9]

$$N_{\mathrm{e}} = N_0 L\left(1 - \frac{1}{\beta^2 n^2}\right)\frac{\varepsilon}{1 - M(1-\varepsilon)}. \tag{5}$$

Aerogel is a unique material that can have a refractive index between those typical for gases and liquids (as small as $n = 1.008$ and as high as $n = 1.094$) [10]. It is a transparent, highly porous $n(\mathrm{SiO_2}) + 2n(\mathrm{H_2O})$ material with a density ranging from $\rho = 0.04$ to $0.20\,\mathrm{g/cm^3}$. The refractive index for the various density aerogel materials is roughly given by

$$n - 1 = (0.210 \pm 0.001)\rho. \tag{6}$$

The optical properties of aerogel can be characterized by an absorption length Λ_{a} and a scattering length Λ_{s}. A typical value of the scattering length, at a wavelength λ of 400 nm, is $\Lambda_{\mathrm{s}} \sim 2$ cm. The absorption length Λ_{a} increases almost linearly in the interval 200–300 nm and remains nearly constant above that. At a wavelength $\lambda \sim 400$ nm, $\Lambda_{\mathrm{a}} \sim 20$ cm [11].

Taking into account the above-mentioned requirements of the Hall C experiments, we chose two different aerogel materials with an index of refraction of $n = 1.030$ and 1.015, respectively.

The threshold momenta P_{th} (in GeV/c) for the particles under consideration in these two types of aerogel materials are presented in Table 1.

In Fig. 1, the expected yields in terms of the number of photo-electrons are given for both types of aerogel (for a thickness ~9 cm and a figure of merit $N_0 \sim 46$), as calculated according to Ref. [12].

It can be seen that the $n = 1.03$ aerogel will allow for good pion/proton separation up to 4 GeV/c, while the $n = 1.015$ aerogel material can be used for pion/kaon separation in the

Table 1
Threshold momenta for the particles in aerogel

Type of particle	P_{th} in $n = 1.030$	P_{th} in $n = 1.015$
μ	0.428	0.608
π	0.565	0.803
K	2.000	2.840
p	3.802	5.379

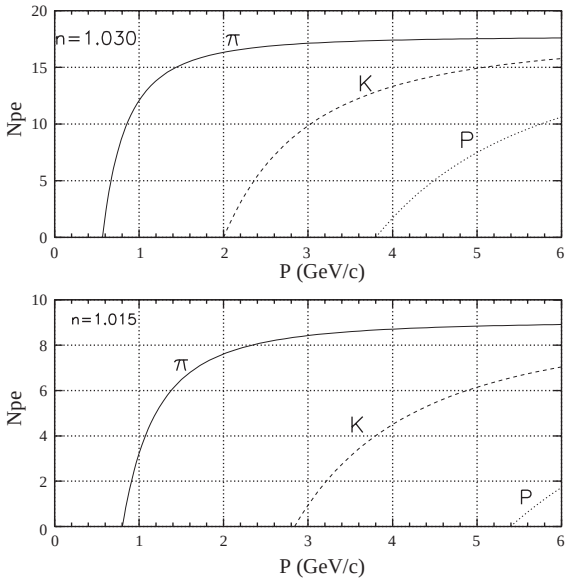

Fig. 1. Particle separation using aerogel Cherenkov with an index of refraction $n = 1.030$ (top) and $n = 1.015$ (bottom). Electrons (positrons) are above threshold over essentially the full momentum range.

momentum range 1–3 GeV/c, and for pion/proton separation up to 6 GeV/c.

Note that the number of photo-electrons (N_{pe}) produced just above the proton (kaon) threshold is much lower for protons (kaons) than for pions, which allows for limited PID just above threshold by counting photo-electrons.

Aerogels commercially available from Matsushita Electric Works Ltd. (Japan) [13] are highly transparent and have a light output which is almost linear with the radiator thickness. They are known to be of high quality. For example, the detailed study of about 1000 tiles of the Matsushita aerogel produced for the HERMES experiment [11] shows that their mean refractive indices are in the $n = 1.0303 \pm 0.0010$ range, with only small variation from tile to tile. Such optical uniformity becomes very important when one needs to obtain the required total thickness about 5–10 cm and to cover an effective detector area $\sim$1 m^2.

The improved light transmittance and hydrophobicity of this "new" aerogel material is due to a new production technique [11,14], and makes it preferable to the early hydrophilic aerogel materials that needed baking and storage in a dry nitrogen atmosphere to maintain the initial good transmittance of the radiator [15] (as was done in the case of Hall C SOS aerogel detector [16]).

Although the light transmittance of aerogel is relatively small, the light absorption is also rather small [11]. Hence, a large number of photons undergo multiple scattering and lose directionality but do eventually reach a photo detector. Diffuse light collection by means of highly reflective walls, also known as a "diffusion box", seems a good choice [17].

3. The aerogel detector

3.1. Physical design

There are different schemes for collecting Cherenkov light. In our detector we make use of a diffusion box. The photon detection probability in the case of a diffusion box is directly proportional to the fraction of detector surface covered by PMTs. An increase in the area covered by PMTs results in an increase of the number of photons detected. Therefore, and based on Monte Carlo calculations, we used 16 PMTs in the counter.

The aerogel detector schematic design is shown in Fig. 2. It is a sandwich of an aerogel tray and a diffusion light box with PMTs. This allows for simple detector assembly and easy replacement of the aerogel stack. The active area is about 120×70 cm^2. Eight PMTs are mounted on both "long" sides of the box. The total area covered by the photo-cathode windows of these PMTs amounts to $\sim$8% of the inner surface of the

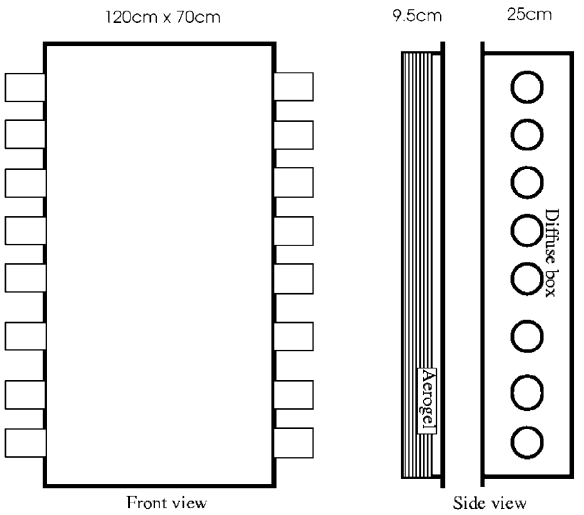

Fig. 2. Schematic drawing of the aerogel detector.

counter. Due to the high reflectivity of the inner walls of the diffusion box, it was covered with Millipore paper "Membrane GSWP-0010" with a reflectivity of ~96% [18].

The simulation for the HMS aerogel detector was done using a dedicated Monte Carlo code [12]. A detector volume (including the aerogel) of $120 \times 70 \times 24.5\,\mathrm{cm}^3$ and 5 in. PMTs with a 20% quantum efficiency were taken.

Several options were considered:

- readout PMTs from one and two sides of the diffusion box;
- 5 and 8 PMTs on each side;
- aerogel thickness of 5 and 9 cm.

As anticipated, the best uniformity of the summed N_{pe} signal (flat within ~10% over the active area of the detector) was found for the two-side readout. The mean number of photo-electrons for a 5 cm thick aerogel of $n = 1.030$ was predicted to be ~6.6 for 10 PMT readout and ~8.3 for 16 PMT readout. For high optical quality of the aerogel material under consideration in the first order, the absorption and scattering of the photons in the aerogel is neglected in the code. This results in a linear increase of the yields with the radiator thickness. Thus, the mean number of photo-electrons for the same type of aerogel of 9 cm thickness was predicted to be ~12.1 for the 10 PMT readout and ~14.8 for the 16 PMT readout. Based on the simulations the final decision was to use 9 cm aerogel with a 16 PMT readout.

Installation of the aerogel detector in the HMS detector stack would alter the PID capacity of the gas Cherenkov located just behind the aerogel due to δ-electron knock-out and multiple scattering.

We estimated that the use of a detector with $n = 1.030$ aerogel material of 9 cm thickness along with entrance and exit windows of total ~2 mm Al thickness would double the number of δ-electrons produced, which could reach ~2% of all particles passing through the HMS detector stack at a momentum $P_{\mathrm{HMS}} \geqslant 4\,\mathrm{GeV}/c$.

We used 16 ten-stage Photonis XP4572B PMTs of 5 in. diameter, with a bialkali photo-cathode and a maximum gain of $\sim 10^7$. These PMTs have a quantum efficiency of ~20% in the wavelength range λ~350–450 nm, which well matches the transmitted radiation spectrum of aerogel. Due to an enhanced photo-electron collection efficiency, the effective number of photo-electrons is increased by a factor of ~2 relative to more commonly used PMTs such as the Burle 8854 as it is claimed in Ref. [20].

The close spacing of the metal shields (to improve the light collection efficiency) required us to keep the cathode at ground potential, while positive high voltage was applied to the anode of the PMT to reduce the noise level. In order to keep dark rates low and prolong the PMTs' lifetime we prefer to operate at lower high voltages. To compensate for the low gain of the chosen PMT at this regime, we modified their high voltage (HV) bases by inserting an amplifier in the HV dividers as a sequential component after the last resistor. The fast amplifier was designed [21] for standby operation at relatively low currents with a signal charge amplification factor of ~10.

Two identical boxes were fabricated for the aerogel trays, one each for the $n = 1.030$ and $n = 1.015$ materials. Both match the common diffusion box and can be easily substituted for each other.

Matsushita produces aerogel in the form of $\sim 110 \times 110 \times 10\,\mathrm{mm}^3$ tiles. In order to stack the material, each tile dimension was first measured

and the differences in block sizes determined. Taking into account the tolerances on the actual aerogel material thickness inside the diffusion boxes, the tiles were layered in 9 stacks in the case of $n = 1.030$ and 8 stacks in the case of $n = 1.015$. In both cases the total thickness of aerogel radiator was 9 cm, using over ~650 tiles for each box. To prevent any stress on the aerogel material from the front side of the detector, the aerogel tiles were stacked on a thin (~5 mm) honeycomb sheet and housed in a tray of dimensions $117 \times 67\,\text{cm}^2$. The layers were shifted relative to each other by about 2–3 cm to prevent any dead zones inside the aerogel volume.

The stacks of aerogel tiles are kept in position by means of a mesh of thin (100 μm) stainless steel wire.

4. Calibration of the photo multiplier tubes

The calibration of a PMT of the aerogel detector consists of the localization of the single photo-electron peak in the ADC pulse height spectrum. The single photo-electron pulse height is used to normalize the PMT raw signal when summing it in the detector response. The detector response, which is the sum of all the PMT signals in photo-electron units, is used eventually in the data analysis.

For the detector to be used in the electronic trigger, it is desirable to have good coordinate uniformity of the summed raw electronic signal. This is accomplished by matching single photo-electron pulse heights by means of high voltage adjustments (“gain matching”).

The preliminary calibration of each PMT was performed by measuring the PMT response to a pulsed light source. The light intensity from the light emitting diode (LED) used was controlled by adjustment of the height and width of the applied pulses. For each PMT, the single photo-electron peak position and its width were found versus the applied high voltage. This allowed us to roughly equalize the response functions for all PMTs, and to determine their gains at a given high voltage.

A preliminary test of the aerogel detector was performed with cosmic rays. The detector was positioned horizontally with the diffusion box on top. A pair of scintillators sandwiched the aerogel detector, with a third one separated by a layer of lead bricks. This lead absorber was used to select the energy of cosmic muons (the threshold momentum of muons firing the $n = 1.030$ aerogel detector is ~430 MeV/c). The DAQ system was a simplified version of the standard DAQ system of Hall C [22]. The cosmic test was used to roughly adjust the PMT high voltages and estimate the number of photo-electrons from cosmic muons. Both a typical pulse height spectrum summed over the 16 tubes, and the single photo-electron positions (in ADC channels) for all the tubes after gain matching, are presented in Fig. 3.

The ability of the aerogel Cherenkov detector to distinguish between cosmic muons above and below detection threshold is illustrated in Fig. 4, where the pulse height spectrum summed over the 16 PMTs is shown for several thicknesses of the lead absorber. The use of the lead absorber between the second and third trigger counters clearly allows the low-energy part of the muon spectrum to be cut off. This is reflected in the

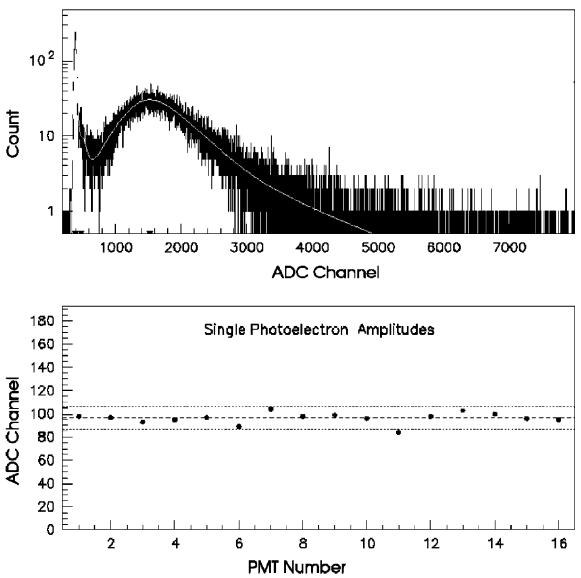

Fig. 3. Pulse height distribution of the total sum of the 16 PMTs (top) and mean value of the single photo-electron signal for each PMT (bottom), from the cosmic test.

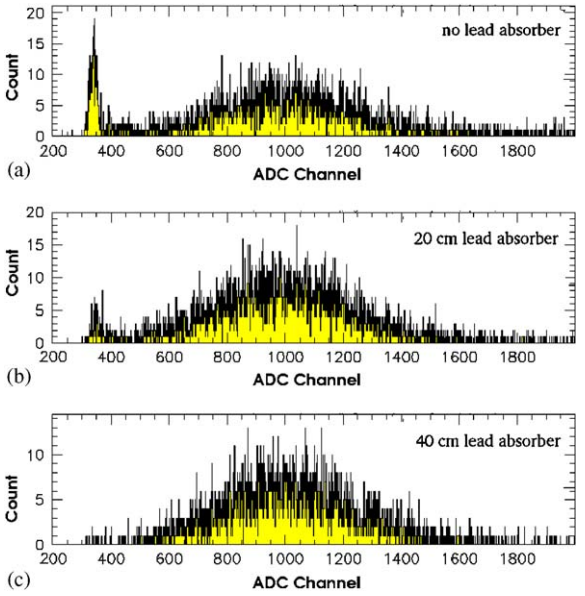

Fig. 4. Cosmic test results for the aerogel detector with $n = 1.030$. The summed pulse height spectrum is shown for various thicknesses of the lead absorber used: (a) no absorber, (b) 20 cm lead (μ momentum $>300\,\mathrm{MeV}/c$), (c) 40 cm lead (μ momentum $P_\mu > 590\,\mathrm{MeV}/c$).

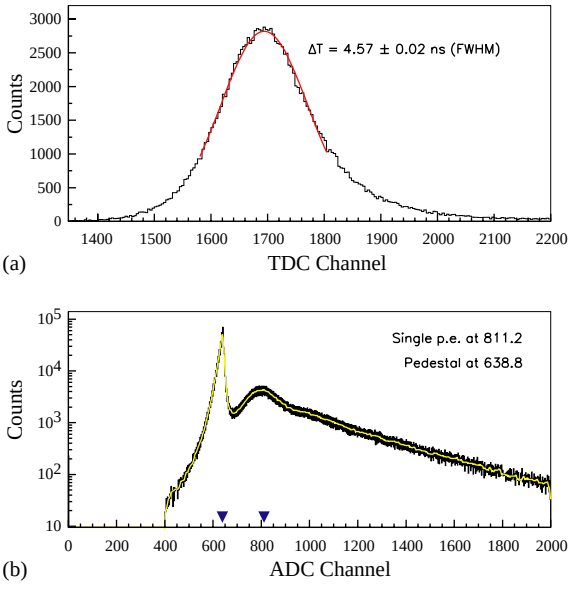

Fig. 5. Typical TDC (top) and ADC (bottom) spectra of an aerogel detector PMT. The smooth lines are Gaussian (TDC) and spline (ADC) fits to the histograms shown. The triangles on the bottom of the ADC spectrum indicate the pedestal and single photo-electron peak positions.

figure as the diminishing of the pedestal events with the increase of the lead absorber thickness.

5. Experimental results with beam

The aerogel detector was installed in the HMS and all PMTs information (ADC and TDC) were integrated into the Hall C data acquisition system, and subsequently successfully used in the Hall C experimental program of 2003. In this section we will show the results obtained with the aerogel detector, for both indices of refraction, with beam.

Fig. 5 shows typical TDC and ADC raw spectra for one of the aerogel PMTs. Although an ~4 ns (FWHM) time resolution is not very good (it is mainly due to the large spread in light paths through the diffusion box), information from the TDC was still useful in the off-line analysis for additional rejection of accidental events in the summed aerogel signal at high rates. One can see a clean separation of the single photo-electron peak from pedestal in the ADC spectrum. The two photo-electron peaks are also, but barely, distinguishable. A smooth fit to such ADC spectra provides pedestal and single photo-electron peak positions for each PMT. These are then used for detector calibration purposes.

In Fig. 6, the distribution of the total number of photo-electrons N_{pe} (for all PMTs summed) for the aerogel detector with $n = 1.015$ (top) and $n = 1.030$ (bottom), respectively, is shown for protons and pions at $3.1\,\mathrm{GeV}/c$. The signal from the pions is nearly in saturation, while the signal from protons at this momentum is still below detection threshold. The mean values of the number of photo-electrons (in saturation) are ~16 for the $n = 1.030$ and ~8 for the $n = 1.015$ aerogels.

The experimental data over a wide range of momenta, from 0.5 to $4\,\mathrm{GeV}/c$, for different types of particles show that the dependence of N_{pe} upon momentum has the expected threshold behavior, and that the number of photo-electrons indeed saturates at high momentum (see Fig. 7).

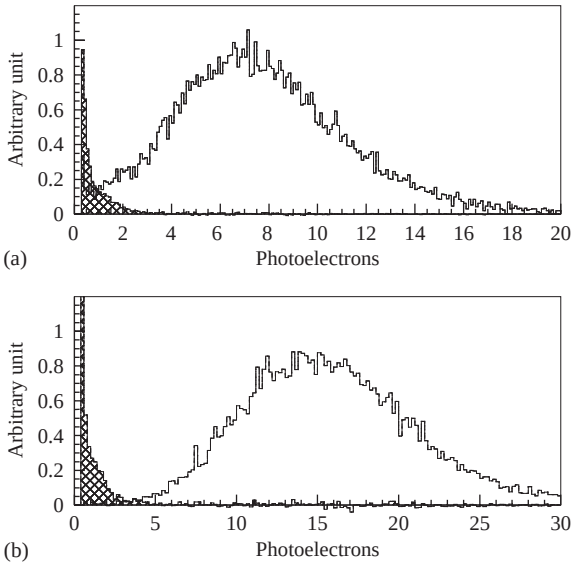

Fig. 6. Total number of photo-electrons for protons (hatched) and pions at $P_{HMS} = 3.1\,GeV/c$ in aerogel with index of refraction of (a) $n = 1.015$ and (b) $n = 1.030$.

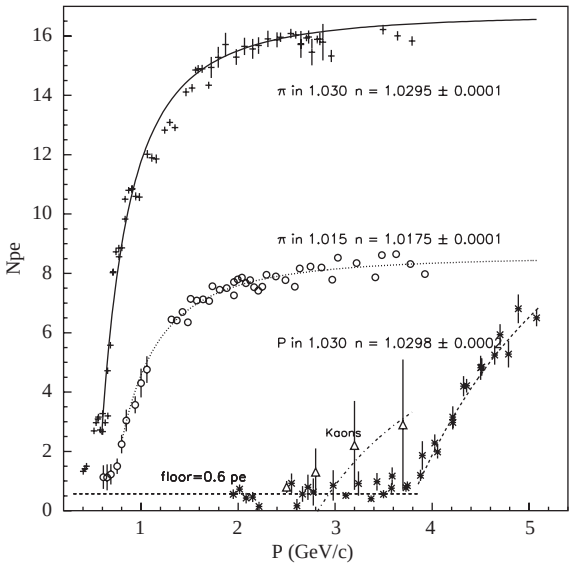

Fig. 7. The momentum dependence of N_{pe} for both types of aerogel material used and for different particles. Both the experimental data and fits to them are shown (compare to Fig. 1).

When the detector is used in threshold mode, or when one would like to estimate the threshold velocity of a particle in the given aerogel (or, alternatively, the index of refraction of the material), it is important to know the response for particles below the Cherenkov threshold. The ~0.6 photo-electron background (for the 16 PMTs summed) shown in Fig. 7 may come from the following sources [19]:

- δ-electrons with momentum above detection threshold;
- accidental events not rejected by the trigger;
- particles causing Cherenkov light or scintillation in the millipore paper or the air in the diffusion box.

After subtraction of this background, one can evaluate the index of refraction of the used aerogel material from a fit to the data shown in Fig. 7. The calculated and real values of index of refraction for both aerogels match well, although better in the case of the aerogel with $n = 1.030$.

From these N_{pe} data, the detector efficiency versus momentum can be determined. This results in an efficiency for pion detection in the aerogel with $n = 1.030$ of more than 99%, in the 1–4 GeV/c momentum range ($N_{pe} \geqslant 4$). For the case of the aerogel material with $n = 1.015$, the pion detection efficiency is more than 97%, assuming a cut level of $N_{pe} \sim 2$, in a 1.2–4 GeV/c momentum range (see Fig. 8).

One of the most important features of any detector is its coordinate dependence of the response function. As shown in Figs. 10 and 11, the total sum of photo-electrons detected by the aerogel detector is nearly flat in both X and Y coordinates. However, its variation from point to point within the acceptance of the spectrometer may be as much as 20% (see Fig. 9; see also Figs. 10 and 11). Not surprisingly, close to the PMTs some enhancement can be seen in the number of photo-electrons detected. Similarly, in Fig. 12 the response function versus the spectrometer fractional momentum deviation ($|\Delta p/p| \leqslant 10\%$) is shown. There is no significant dependence over the full momentum acceptance of the HMS.

Note that for these last cases a cut of $N_{pe} > 4$ was used to provide more than 99% detection efficiency for the ($n = 1.030$) aerogel detector. The aerogel material with index of refraction ($n = 1.015$) shows

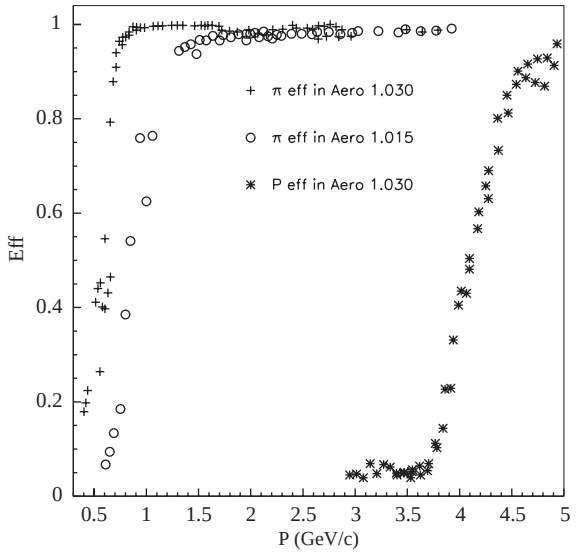

Fig. 8. Particle detection efficiency versus momentum P for the detector with aerogels $n = 1.030$ and $n = 1.015$.

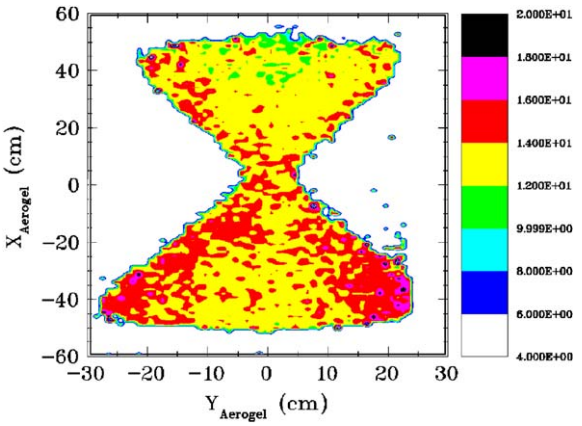

Fig. 9. N_{pe} two-dimensional distribution on the aerogel detector surface for pions in $n = 1.030$ aerogel at 3.336 GeV/c. An "hour-glass" shape of the impact point distribution comes from point-to-point tune of the magnetic optics of the HMS.

a similar behavior, but with less detection efficiency (97% for an $N_{pe} > 2$ cut condition).

The long-term stability of the HMS aerogel detector was tested during experimental runs in Hall C over a 6-month period. The mean number of photo-electrons for the summed detector signals remained stable to within ~2%, with a typical particle rate of ~500–600 kHz.

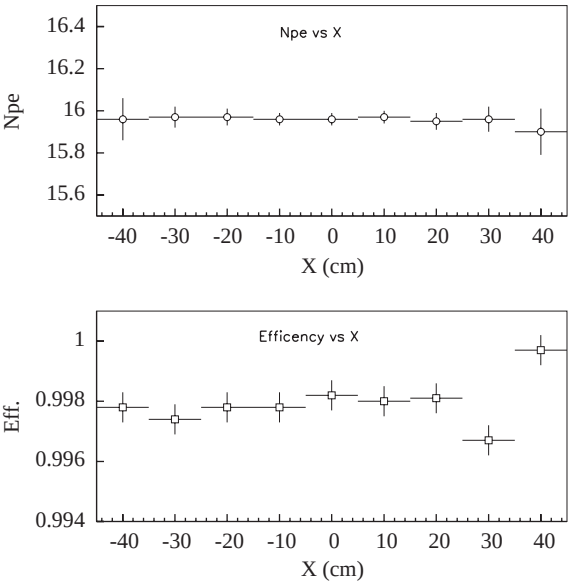

Fig. 10. N_{pe} distribution (top) and pion detection efficiency (bottom) at 4 p.e. threshold versus the vertical X-coordinate (for the detector with aerogel $n = 1.030$) at $P_\pi = 3.2$ GeV/c.

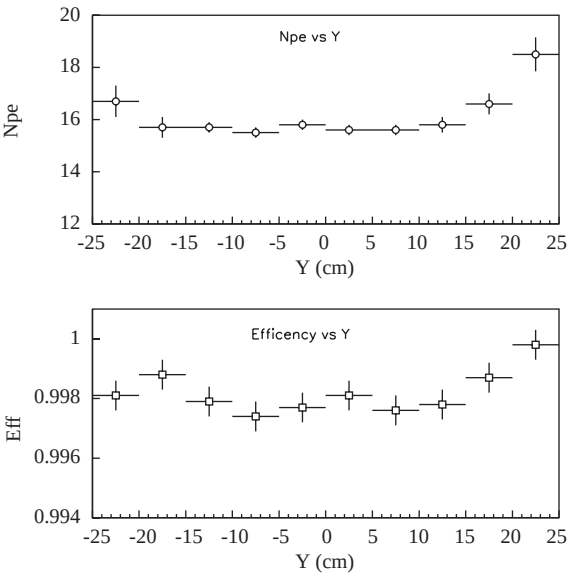

Fig. 11. N_{pe} distribution (top) and pion detection efficiency (bottom) at 4 p.e. threshold versus the horizontal Y-coordinate (for the detector with aerogel $n = 1.030$) at $P_\pi = 3.2$ GeV/c).

Our studies show that, for an aerogel detector with $n = 1.015$ (where kaons cross detection threshold at a momentum of 2.8 GeV/c), it is more

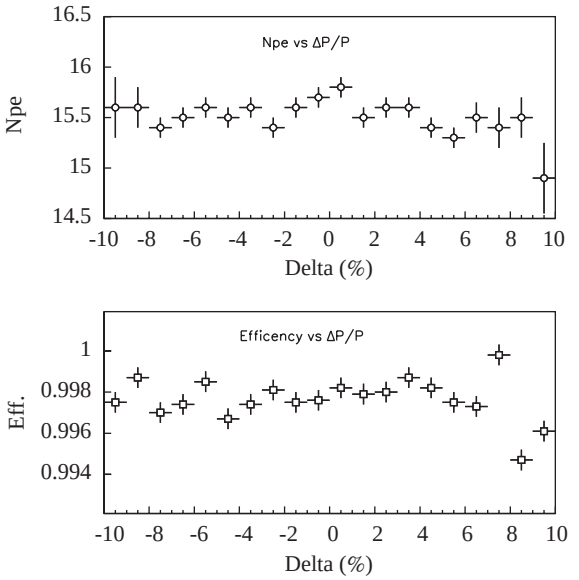

Fig. 12. N_{pe} distribution (top) and pion detection efficiency (bottom) at 4 p.e. threshold versus HMS fractional momentum deviation (for the detector with aerogel $n = 1.030$).

efficient to use the aerogel detector to reject kaons than to select them. The number of photo-electrons generated by these kaons is about 4 at a momentum 4 GeV/c, as shown in Figs. 1 and 7. The fraction of kaons above 2 photo-electron threshold is ~95% at $P = 3.7$ GeV/c, and only ~6% at 2.4 GeV/c.

6. Conclusions

The particle identification properties of the HMS in Hall C at Jefferson Lab have been significantly improved by adding a flexible aerogel threshold Cherenkov detector. The detector consists of an aerogel material followed by a light diffusion box. The radiator tray can easily be swapped for an alternate one with aerogel material with different index of refraction. The addition of this detector enhanced the capabilities of the spectrometer in distinguishing protons from pions on the level of $2.8–1.1 \times 10^{-3}$ (for aerogel with $n = 1.030$) with a pion detection efficiency better than 99% in the 1–4 GeV/c momentum range. It allowed the distinction of kaons from pions on the level of 10^{-2}, for aerogel with $n = 1.015$, with a pion detection efficiency better than 97% in a 1.2–4 GeV/c momentum range. The mean numbers of detected photo-electrons are ~16 and ~8 for the $n = 1.030$ and $n = 1.015$ aerogel material, respectively. The detector response is uniform to within ~10% over the full effective area. The experimental results are in good agreement with expected values from simulations using a standard Monte Carlo program for aerogel detectors [12]. The number of fake photo-electrons for particles below detection threshold reaches ~0.6, which may be a result of δ-electrons, accidental events or scintillation of particles traversing the detector.

Acknowledgements

We wish to thank many people who assisted and contributed in the design, construction and testing of this detector. We are particularly indebted to R. Carlini for support to construct such a detector, D. Higinbotham for assistance and providing access to his Monte Carlo simulation program for aerogel detectors, B. Wojtsekhowski for interest and many useful discussions, C. Zorn for valuable contributions to the systematic tests of the PMTs, V. Popov for the development of the PMT amplifier and the installation of these in the HV bases, W. Kellner and his group for their technical expertise and help with the installation of the aerogel detector and the aerogel radiator replacement in Hall C. Lastly, many thanks to J. Beaufait for continuous help during all stages of the construction and the preliminary testing.

The Southeastern Universities Research Association (SURA) operates the Thomas Jefferson National Accelerator Facility for the United States Department of Energy under contract DE-AC05-84ER40150.

References

[1] CEBAF, Conceptual design report—basic experimental equipment, Newport News, Virginia, April 13, 1990.
[2] P. Bosted, V. Frolov, M. Jones, V. Koubarovski, P. Stoler, spokespersons, TJNAF Experiment E01-002.

[3] H. Blok, G. Huber, D. Mack, spokespersons, TJNAF Experiment E01-104.
[4] R. Ent, H. Mkrtchyan, G. Niculescu, spokespersons, TJNAF Experiment E00-108.
[5] D. Cantin, et al., Nucl. Instr. and Meth. 118 (1974) 177.
[6] P.A. Cherenkov, Phys. Rev. 52 (1937) 378.
[7] I.E. Tamm, I.M. Frank, Dokl. Akad. Nauk SSSR 14 (1937) 107.
[8] G. Poelz, Nucl. Instr. and Meth. A 248 (1986) 118.
[9] P. Carlson, Nucl. Instr. and Meth. A 248 (1986) 110.
[10] H. Yokogawa, M. Yokoyama, J. Non-Cryst. Solids 186 (1995).
[11] E. Aschenauer, N. Bianchi, G. Capitani, et al., Nucl. Instr. and Meth. A 440 (2000) 338.
[12] D. Higinbotham, Nucl. Instr. and Meth. A 414 (1998) 332.
[13] Matsushita Electric Works, 1048 Kadoma, Kadoma-shi, Osaka 571, Japan.
[14] I. Adachi, et al., Nucl. Instr. and Meth. A 355 (1995) 390.
[15] S. Henning, L. Svensson, Phys. Scripta 23 (1981) 697.
[16] R. Mohring, Ph.D. Thesis, University of Maryland, 1999, and http://www.jlab.org/Hall-C.
[17] M. Benot, et al., Nucl. Instr. and Meth. 154 (1978) 253.
[18] Millipore Corporation, 80 Ashly Road, Bedford, MA, http://www.millipore.com.
[19] D. Barancourt, et al., Nucl. Instr. and Meth. A 465 (2001) 306;
Y. Asaoka, et al., Nucl. Instr. and Meth. A 416 (1998) 236.
[20] B. Wojtsekhowski, C. Zorn, S. Flyckt, Nuclear Science Symposium Conference Record, vol. 1, 15–20 October. 2000, IEEE, Lyon, France, pp. 7/63–7/65.
[21] V. Popov, et al., Nuclear Science Symposium Conference Record, vol. 2, 4–10 November 2001, IEEE, San Diego, California, USA, pp. 634–637.
[22] Hall C Analysis Documentation, http://www.jlab.org/Hall-C.